

## Double electron capture in $\text{Ne}^{8+}$ -He collisions at intermediate energies

M. L. A. Raphaelian,\* H. G. Berry, and N. Berrah†

*Physics Division, Argonne National Laboratory, Argonne, Illinois 60439*

D. Schneider

*High Temperature Physics Division, Lawrence Livermore Laboratory, P.O. Box 808, Livermore, California 94550*

(Received 4 February 1993)

High-resolution Auger spectra of doubly excited Be-like neon have been obtained for intermediate collisional velocities (0.89–1.79 a.u.).  $\text{Ne}^{8+}$  was produced at high voltage in the Argonne National Laboratory electron-cyclotron-resonance ion source. A differentially pumped helium gas cell was used to study double electron capture. The *LMX* Auger decays of the Be-like neon are observed with a high-resolution  $0^\circ$  tandem electron spectrometer. High-angular-momentum states are observed to be populated during the collisions and their relative amplitudes change dramatically with increasing collisional velocity.

PACS number(s): 34.50.Fa, 34.70.+e, 32.80.Dz

### I. INTRODUCTION

Investigations involving multielectron transfer during collisions between highly charged ions and atoms have been performed by several groups (Bordenave-Montesquieu *et al.* [1], Mack *et al.* [2], Moretto-Cappelle *et al.* [3], Boudjema *et al.* [4], Rocin, Barat, and Larent [5], and Barat and Rocin [6], and references therein). These previous experiments have involved projectiles with collisional velocities well below one atomic unit of velocity. During the collision the target electrons tend to be captured sequentially into equivalent or nearly equivalent energy quantum levels, leaving the projectile in a doubly or multiexcited state. The relaxation of the projectile proceeds by Auger decay or radiative stabilization. Using high-resolution Auger spectroscopy, the multiexcited state in the projectile can be identified and the results can be compared quantitatively with theoretical models for multielectron capture. In this paper, we present such measurements of two-electron capture and subsequent Auger decay over significant projectile velocity ranges.

Classical models involving independent electrons can describe the main features observed in such high-resolution Auger spectra. In particular, the extended over-barrier model (Niehaus [7]) does quite well in the description of which principal quantum number  $n$  levels are populated in the projectile during the capture process and the estimate of the multielectron capture cross section. These over-barrier models, however, do not incorporate any velocity dependence of the capture cross section or the angular momentum distribution of the captured electrons. Extensions of the model to include the angular momentum distributions have had little success in the description of what is observed spectroscopically. Recently Posthumus, Lukey, and Morgenstern [8] using the extended over-barrier model have had some success in describing the angular momentum distribution for double electron capture for bare projectiles, but less suc-

cess for double electron capture in He-like projectiles. All their measurements were made at very low projectile velocities  $v_p \ll 1$  a.u., where the postulates in the classical overbarrier models are presumed to be valid.

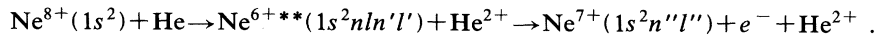
Quantum models using a two-center atomic orbital close-coupling expansion have been performed by Chen and Lin [9] on the system presented in this paper. In their treatment, they choose the quantization axis of the manifold to be perpendicular to the scattering plane. The probability for capture into a specific single-electron configuration is then calculated as a function of impact parameter for each electron captured. The convolution of these probabilities gives the total probability for capture into a multiexcited configuration of the projectile. They have also shown that most of the Auger flux is directed into the forward  $0^\circ$  laboratory direction. These calculations provide a basis for comparing our measured velocity-dependent cross sections and the individual angular momentum of the excited states.

In this study we have measured the electron spectra for the  $\text{Ne}^{8+} + \text{He}$  collisional system at the somewhat higher velocities of 0.89, 1.27, 1.55, and 1.790 a.u. We have used the technique of high-resolution  $0^\circ$  electron spectroscopy to observe the angular momentum distributions produced during these collisions for the doubly excited states in the  $(3l3l')$ , and  $(3l4l')$  manifolds of  $\text{Ne}^{6+}$ . Velocity-dependent studies of this nature can help in understanding the dynamics of ion-atom collisions. Unlike the slow collisions previously studied, the doubly excited state in the projectile has less time to interact with other nearby lying levels within the given manifold before the projectile relaxes by Auger decay. As the collisional velocity decreases, the states within a given doubly excited manifold have more time to interact leading to a redistribution of angular momentum in the system and the observed spectra may no longer represent the original double capture configurations. By studying the velocity dependence of a collisional system, the dynamical effects of the projectile-target system on the angular momentum distribution within the projectile are measured.

## II. EXPERIMENT

The  $\text{Ne}^{8+}$  ions were produced in the positive-ion injector electron cyclotron resonance (ECR) source at the Argonne Tandem/LINAC (linear accelerator) Accelerator System (ATLAS) facility of Argonne National Laboratory [10]. The extraction voltage from the ion source can be varied from 10 to 15 kV and for this experiment was set to a value of 12 kV. This ECR ion source is located on a 350-kV platform. The platform potential can also be varied thus giving the experimenter a wide choice of energy for the ion-atom collision. In this experiment the platform voltage was varied to give collisional energy per charge of 50–200 keV in steps of 50 keV.

The He-like neon ions were extracted from the source, charge-to-mass analyzed by a 90° magnet, accelerated, and delivered to the atomic physics beam line. Figure 1 shows in detail the low-energy atomic physics beam lines



The gas target cell consisted of an electrically isolated entrance and exit aperture, an electrically isolated 76.2-mm cylindrical aluminum cell, and a glass ion gauge connected to the cell. The glass ion gauge allowed us to observe the pressure within the cell before and after each run. For this experiment the gas pressure in the target cell was maintained at 40  $\mu\text{Torr}$ . The cell body was biased to  $-50$  V during the experiment thereby discriminating against capture events outside the target region.

The projectile Auger electrons and the projectiles then entered a 0° tandem electron spectrometer, where the electrons were energy analyzed. The electron spectrometer consisted of two sequential 45° parallel plate spectrometers of dimensions 100.0 mm in length, 43.9 mm in width, and 20.3 mm in height. The top plate of the first low-resolution spectrometer has a 6.4-mm-diam hole to allow passage of the ion projectiles through to the Fara-

day cup. The ion beam was collimated before entering a magnetically shielded electron-scattering chamber. This was accomplished by the use of three sets of four-jaw slits in the beam line and a 2-mm-diam collimator at the entrance to the scattering chamber.

Typical analyzed beam currents before entering the scattering chamber were 1.25, 1.5, 2.0, and 2.5  $\mu\text{A}$  for the 20-, 40-, 60-, and 80-keV/amu runs. In the scattering chamber, typical beam currents were 20, 40, 95, and 140 nA, respectively. The beam-line residual pressure and the scattering chamber residual pressure were both less than 0.4  $\mu\text{Torr}$ , ensuring purity of the projectile charge state into the target interaction region.

Once in the scattering chamber, the collimated  $\text{Ne}^{8+}$  ion beam entered a differentially pumped helium gas target cell where the double-electron-capture process occurs. For He-like neon on a helium target, the double-electron-capture process is as follows:

day cup. The low-resolution spectrometer entrance and exit slit dimensions were 10 mm in length by 2 mm in width. The second parallel plate spectrometer, provides high resolution and has entrance and exit slits of 5 and 0.5 mm respectively. The calculated acceptance angle with respect to the ion-beam direction equals  $\theta = 0.00^\circ \pm 0.72^\circ$ , which gives an energy resolution of  $\Delta E/E \leq 2 \times 10^{-2}$ . The spectrometers were mounted in tandem and operated in constant pass energy mode, such that the energy-analyzed electrons from the low-resolution spectrometer were decelerated to 10 V of energy before they entered the high-resolution spectrometer. Electrons which were analyzed by the spectrometer were then detected by a channeltron. A linear dependence of the signal was observed with pressure variation ensuring that the observed spectra were due to single collision events. The undeflected ion beam was collected at the

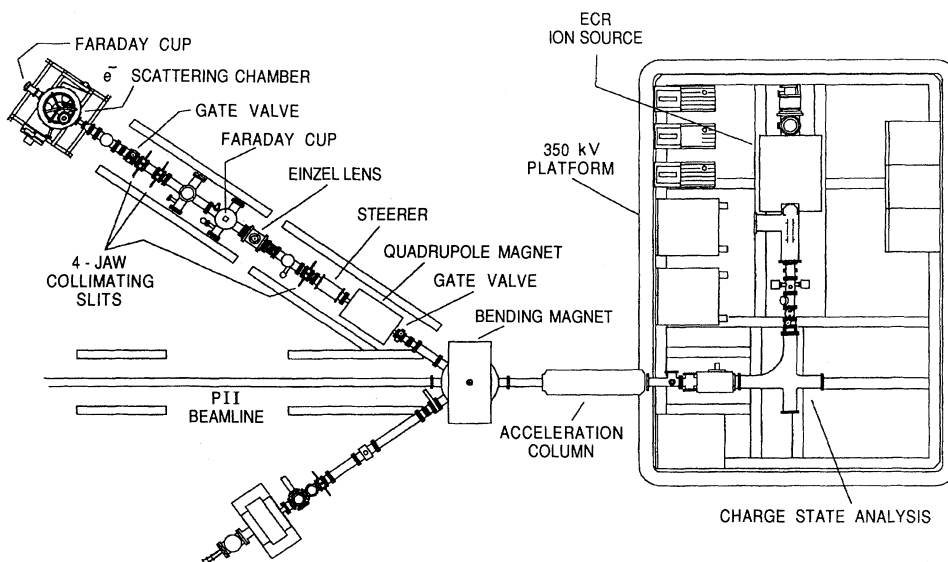


FIG. 1. The low-energy atomic-physics beam lines at the ATLAS facility.

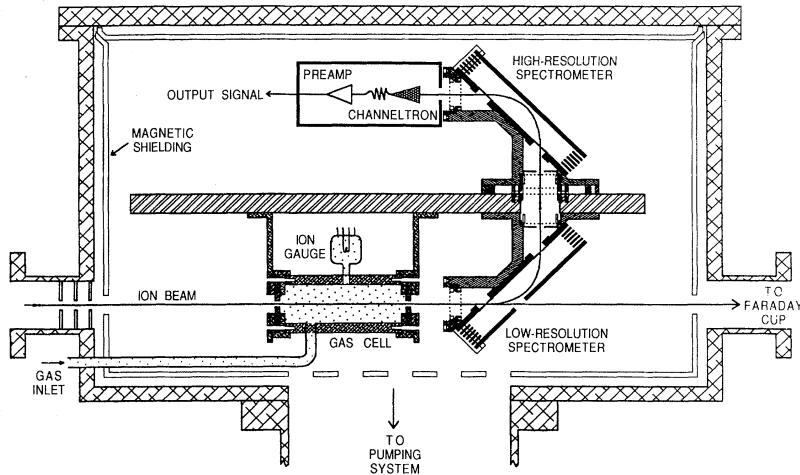


FIG. 2. The  $e^-$  scattering chamber and  $0^\circ$  tandem electron spectrometer. Attached to the target gas cell is a glass ion gauge which allows the target pressure to be monitored before and after each run.

back of the scattering chamber in a Faraday cup. The measured Faraday cup current was integrated and used for normalization such that each channel in the spectrum has the same collected charge from the Faraday cup. The scattering chamber and spectrometer setup are shown in Fig. 2. The electron spectra shown in the following section have been transformed into the emitter, projectile frame.

### III. RESULTS

Experimental results for the system  $\text{Ne}^{8+} + \text{He}$  have been obtained (Boudjema *et al.* [4]) at the collisional velocity of 0.40 a.u. They observed the projectile Auger electrons emitted at laboratory angles of  $10^\circ$ ,  $90^\circ$ , and  $160^\circ$ . They also observed that the amplitudes of the Auger decays vary with observation angle. This effect has also been observed by Holt *et al.* [11] in the collisional system  $\text{C}^{5+} + \text{He}$ . In their experiment they observed the carbon Auger spectra from double-electron capture at

nine angles and at four low collisional velocities from 0.29 to 0.50 a.u. They showed that the population of the odd angular momentum and odd  $m_l$  substates increased while that of the even angular momentum and even  $m_l$  substates decreased with increasing collisional velocity. The angular momentum distributions of projectile Auger electrons were also analyzed by Mack *et al.* [2] in the collisional systems of  $\text{C}^{6+} + \text{H}_2$  at 0.43 a.u. and  $\text{O}^{8+} + \text{H}_2$  at 0.46 a.u. at  $50^\circ$ . In this study he found that in the doubly excited  $3/3l'$  configurations, the largest angular momentum state available to the system, the  $^1G$  configuration, was predominantly populated with the percentages of 55% and 48%, respectively. The second largest angular momentum state available to the system, the  $^1F$  configuration, contributed to 8% and 9% of the total Auger emission, while the  $^1D$  configurations ranged from 6% to 12% and 4% to 14%, respectively, for the two cases.

The Auger spectra produced by double electron capture in this collision are dominated by  $LMX$  Auger decays, where  $X$  is  $M, N, O$ , and  $P$ . These states are identified in Fig. 3. Since each doubly excited state can decay into either the  $2s$  or  $2p$  final state, there are two transitions for each doubly excited state. The  $2p$  final

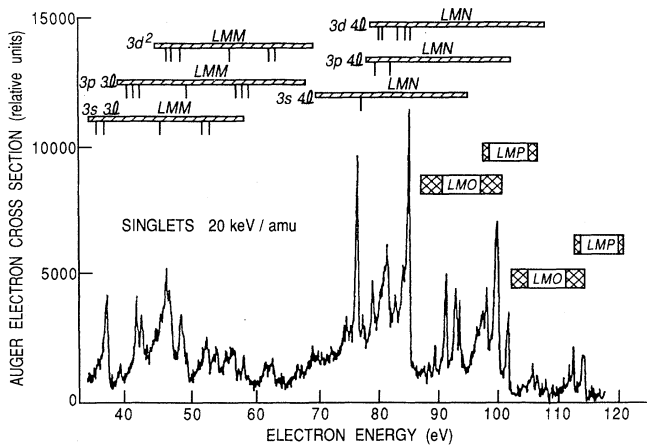


FIG. 3. The  $LMX$  Auger spectra for the collisional energy of 20 keV/amu. The doubly excited manifolds overlap in energy. The decay into the final-state configuration of  $1s^2 2p$  produces Auger electrons of less energy than the decay into configuration  $1s^2 2s$ .

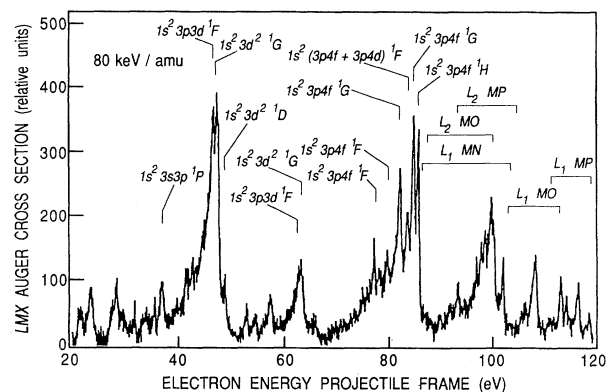


FIG. 4. Spectroscopic identification of some of the observed Auger lines for the collisional energy of 80 keV/amu. At these high collisional energies the highest-angular-momentum states available to the system dominate the spectrum.

configuration leads to electrons of lower energy. As can be seen from this figure, the energies of the doubly excited configurations overlap with one another, thereby making identification difficult for some of the higher energy lines. Figure 4 indicates our identification for some of the transitions.

Figure 5 shows the progression of the Auger spectra with increasing collisional energy. This identification of the dominant lines observed in the spectra was accomplished by comparison with our calculations of the theoretical energies. Certain features of the spectra become apparent with increasing collisional energy. The reduction in the Auger yield is due to the decreasing capture cross section as the velocity of the collision increases. Another important and immediate observation is the decrease of the  $3l4l'$  population and increase in the  $3l3l'$ ,  $3l5l'$ , and  $3l6l'$  populations with projectile velocity. This feature can be explained in the extended over-barrier model from the broadening of the reaction window for capture. The most striking observation however is that the angular momentum distribution within a given  $3lnl'$  manifold changes dramatically as the collisional ve-

locity increases: as can be seen in Fig. 5 certain angular momentum states observed in the 20-keV/amu collision disappear from the spectrum at the collisional energy of 80 keV/amu. At the lower collisional energies, all the singlet configurations contribute to the Auger spectra. However, as the projectile energy increases, the  $^1S$ ,  $^1P$ , and  $^1D$  Auger amplitudes decrease relative to the  $^1F$  and  $^1G$  amplitudes in the  $3l3l'$  manifold. The dominant  $3l3l'$  singlet states at the highest collisional energy are due to the  $3p3d^1F$  and  $3d^2^1G$  doubly excited configurations. In the  $3l4l'$  manifold, the singlet states with the high-angular-momentum values are also observed to be stronger at all collisional energies than those with lower values. In Fig. 6 we present the Auger spectra for the highest collisional energy studied in this experiment and compare it with the theoretical spectra calculated for this collisional system by Chen and Lin [9]. The experimental spectra and the calculated theoretical spectra agree at this collisional energy. At lower collisional energies the agreement between theory and experiment is still good, but the theory underestimates the low-angular-momentum contributions to the Auger flux (Fig. 7).

The total cross section for double electron capture decreases with increasing collisional velocity. Some individual doubly excited configuration cross sections decrease faster relative to others. This is due to the interactions between the final states in the doubly excited configuration before the decay takes place. Table I summarizes the relative cross sections for the observed Auger

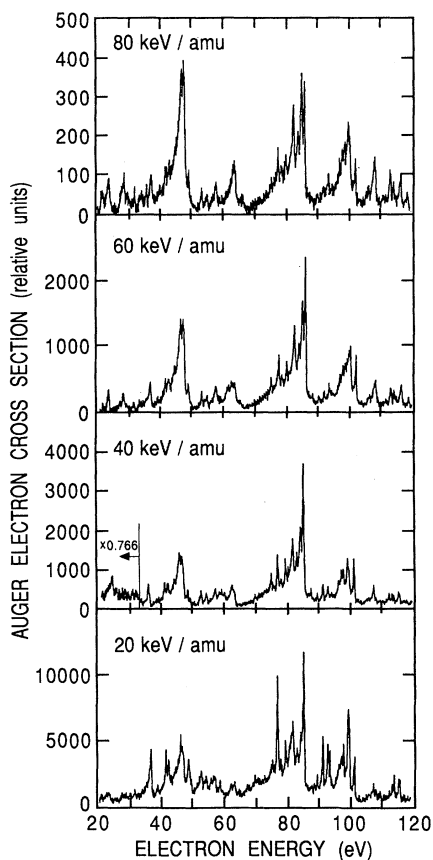


FIG. 5. The progression of the Auger electron spectra with increasing collisional energy. The low-angular-momentum states observed in the 20-keV/amu collision have disappeared in the 80-keV/amu collision. The progression shows that dynamical effects of the collision are important in which states are populated during double electron capture.

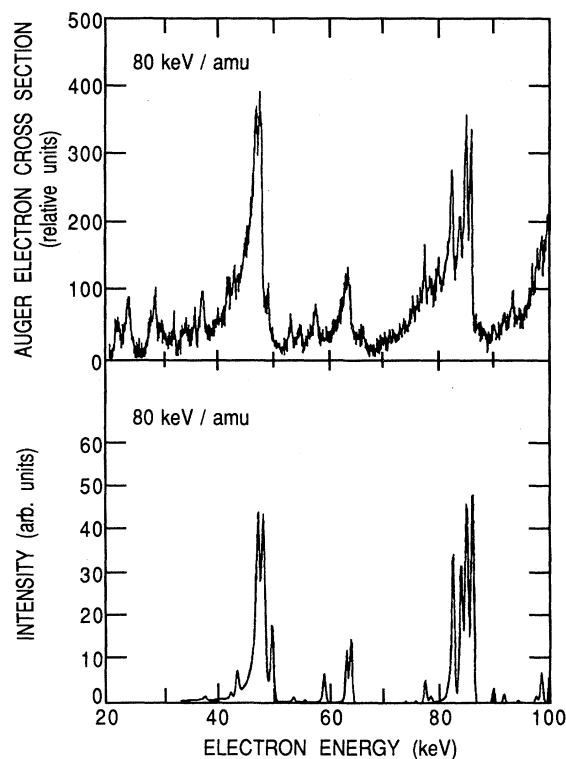


FIG. 6. Comparison of experimental spectra with theoretical spectra for the collisional energy 80 keV/amu.

TABLE I. Relative Auger electron flux into different energy regions for each of the four experimental collisional energies studied in this experiment.

Auger energy range (eV)	Projectile energy (keV/amu)			
	20	40	60	80
35-38	0.034	0.024	0.026	0.020
38-51	0.160	0.184	0.216	0.246
51-69	0.114	0.118	0.115	0.117
69-89	0.390	0.412	0.367	0.309
89-104	0.224	0.180	0.182	0.188
104-120	0.078	0.082	0.094	0.120
35-120	1.000	1.000	1.000	1.000

electron production in certain energy regions. These relative cross sections are normalized with respect to the total yield at each collisional energy. In this table, the yields are broken into six energy regions. Each of these regions contain major features of the spectra. In the first region, the major feature is the decay into the  $2p^2P$  state from the configuration  $3s3p^1P$ . The second region contains predominantly decays from the  $^1F$  and  $^1G$  configurations and the less strong  $^1S$ ,  $^1P$ , and  $^1D$  configurations. The third region contains the remainder of the singlet states and decays into the  $1s^2s$  final-state configuration. Effectively, the first three regions

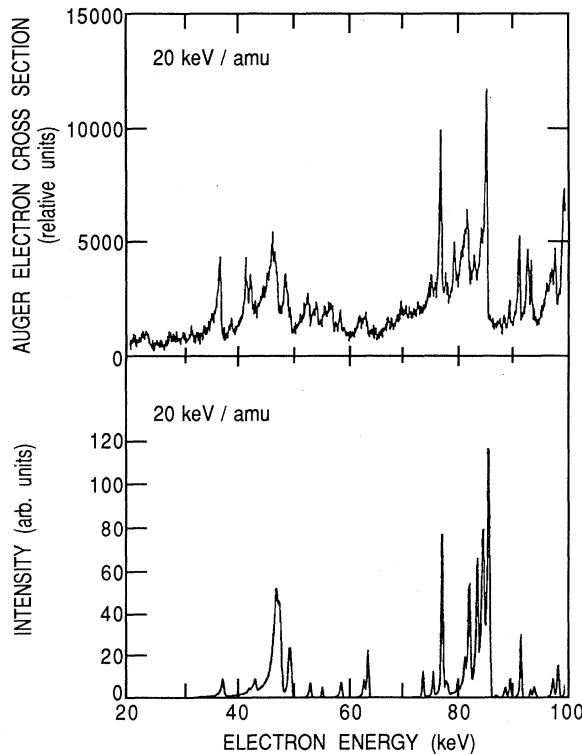


FIG. 7. Comparison of experimental spectra with theoretical spectra for the collisional energy 20 keV/amu.

TABLE II. Total relative *LMX* Auger electron cross section for each of the collisional energies studied.

Projectile energy (keV/amu)	Relative cross section
20	2040
40	550
60	460
80	110

represent the total relative cross section for double electron capture into the  $3/3/1'$  for this collisional system. The fourth region contains most of the major features of the *LMN* spectra. The fifth region occurs where the *LMN*, *LMO*, and *LMP* Auger decays overlap. For the *LMO* and *LMP* Auger decays, the final state of the projectile is  $1s^22p$  while for the *LMN* decays it is the  $1s^22s$  state. The last division occurs also for the *LMO* and *LMP* Auger decays in which the final state is the  $1s^22s$  state.

Certain trends as the energy increases are easily seen from this table. The production of the doubly excited  $3/3/1'$  states increases from 31% to 38%, while the production of the doubly excited  $3/4/1'$  configurations decreases from over 50% of the total yield to less than 40%. The production of the excited  $3/5/1'$  and  $3/6/1'$  states increases from under 20% to around 25% of the total yield at 80 keV/amu. At the lowest collisional energy, the  $3/3/1'$  configuration decays into the  $2p^2P$  final state is 63% of the time and 37% goes into the  $2s^2S$  state. At the highest collisional energy it is 79% and 21%, respectively. Using these percentages to estimate the amount of *LMO* and *LMP* fluxes into the  $2s^2S$  state, we find 8.3% and 3.9%. The estimate for the lower collisional energy agrees well with the observed value of 7.8%. For the flux into the doubly excited  $3/4/1'$  configuration we find 14.4% and 6.5%, respectively. Again, as with the above case for *LMO* and *LMP*, the estimate of 14.4% is consistent. For the highest collisional energy, this estimate is off by a factor of 3. The estimate for the higher-energy collisions fail due the production of *LMM* electrons which decay into the  $2s^2S$  final state which remains a constant percentage at all collisional energies. However, the production of the other Auger electron states change with energy. Table II outlines the total relative cross section as a function of energy for the *LMX* Auger electrons.

#### IV. CONCLUSIONS

We have studied the process of double electron capture of  $\text{Ne}^{8+} + \text{He}$  over a wide range of collisional energies not previously studied. We have shown that the production of the various angular momentum states within a manifold varies greatly with collisional velocity, in contrast to the generally used semiclassical models for these collisions. To understand the dynamics of electron capture processes, velocity-dependent studies of this nature are important. We have observed the production of high-angular-momentum states in the projectile. At lower col-

lisional velocities, most angular momentum states of the doubly excited configuration are observed. At the highest collisional velocity the highest-angular-momentum states dominate the spectra. The production of these states at the higher collisional velocities can be explained by the two-center atomic orbital close coupling expansion method by Chen and Lin [9]. We have also observed that the Auger flux of the *LMN* electrons decreases and the production of *LMM* Auger electrons increases with increasing collisional velocity.

#### ACKNOWLEDGMENTS

This work was supported by the U.S. Department of Energy, Office of Basic Energy Sciences under Contract No. W-31-109-ENG-38. We wish to thank R. C. Pardo and P. Billquist for the use of the ECR ion source. We also wish to thank C. Kurtz, R. Vondrasek, and B. J. Zabransky for the technical help provided. We wish to thank Z. Chen and C. D. Lin for many helpful discussions.

---

\*Present address: Kansas State University, Manhattan, KS 66506.

†Present address: Western Michigan University, Kalamazoo, MI 49008.

- [1] A. Bordenave-Montesquieu *et al.*, *J. Phys. B* **20**, L695 (1987).
- [2] M. Mack *et al.*, *Phys. Rev. A* **39**, 3846 (1989).
- [3] P. Moretto-Cappelle *et al.*, *J. Phys. B* **22**, 271 (1989).
- [4] M. Boudjema *et al.*, *J. Phys. B* **24**, 1695 (1991).
- [5] P. Rocin, M. Barat, and H. Laurent, *Europhys. Lett.* **2**, 371 (1986).
- [6] M. Barat and P. Rocin, *J. Phys. B* **25**, 2205 (1992).
- [7] A. Niehaus, *J. Phys. B* **19**, 2925 (1986).
- [8] J. H. Posthumus, P. Lukey, and R. Morgenstern, *J. Phys. B* **25**, 987 (1992).
- [9] Z. Chen and C. D. Lin, following paper, *Phys. Rev. A* **48**, 1298 (1993).
- [10] R. W. Dunford *et al.*, *Nucl. Instrum. Methods Phys. Res. Sect. B* **40/41**, 9 (1989).
- [11] R. A. Holt *et al.*, *Phys. Rev. A* **43**, 607 (1991).